C. R. Physique 14 (2013) 27–38

Contents lists available at SciVerse ScienceDirect

Comptes Rendus Physique

www.sciencedirect.com

Physics in High Magnetic Fields / Physique en champ magnétique intense

Quantum vacuum magneto-optics

Magnéto-optique du vide quantique

Rémy Battesti, Paul Berceau, Mathilde Fouché, Geert L.J.A. Rikken, Carlo Rizzo *

Laboratoire national des champ magnétiques intenses (UPR 3228, CNRS-UPS-UJF-INSA), 31400 Toulouse, France

ARTICLE INFO

Article history:
Available online 20 September 2012

Keywords:
Intense magnetic field
Quantum electrodynamics
Cotton–Mouton effect

Mots-clés :
Champ magnétique intense
Électrodynamique quantique
Effet Cotton–Mouton

ABSTRACT

In this article we report on the recent experimental activities concerning the magneto-optics of quantum vacuum performed by our team based at the LNCMI of Toulouse. In particular, we will deal with quantum vacuum Cotton–Mouton and inverse Cotton–Mouton effects which have been predicted in the framework of Quantum electrodynamics. Finally, we will present our experiment on photon oscillations into massive particles in the presence of a magnetic field, an effect that could be a signature of physics beyond the standard model.

RÉSUMÉ

Dans cet article, nous décrivons nos récentes activités de recherche sur l'étude des effets magnéto-optiques du vide quantique, réalisées par notre équipe au LNCMI de Toulouse. En particulier, nous présenterons les effets Cotton–Mouton et Cotton–Mouton inverse du vide quantique qui ont été prédits dans le cadre de la théorie de l'électrodynamique quantique. Nous terminerons par la présentation de notre expérience sur la recherche d'oscillations de photons en particules massives en présence d'un champ magnétique, un effet qui pourrait être une signature de physique hors modèle standard.

1. Introduction

In classical electrodynamics vacuum electromagnetic properties are simply represented by two fundamental constants: the vacuum permittivity ϵ_0 and the vacuum permeability μ_0, the value of which has to obey to the fundamental relation $c = \frac{1}{\sqrt{\epsilon_0 \mu_0}}$ with c the speed of light in vacuum. The constant ϵ_0 is the proportionality factor between D and E, while μ_0 is the proportionality factor between B and H. Any variation of the speed of light is ascribed to the fact that light is propagating in a medium, i.e. not in vacuum. To describe such a phenomenon, one introduces the constants ϵ and μ, the value of which characterizes the medium itself. The speed of light in a medium is smaller than the one in vacuum by a factor n, the index of refraction, with $n = \frac{\sqrt{\epsilon\mu}}{\sqrt{\epsilon_0\mu_0}}$. Vacuum is therefore the medium to which, in classical electrodynamics, we associate an index of refraction n exactly equal to 1.

Since the middle of the XIX century, when Faraday discovered that an external magnetic field could change the polarization of light propagating in matter because of a magnetically induced circular birefringence [1], it is known that the

* Corresponding author.
E-mail address: carlo.rizzo@lncmi.cnrs.fr (C. Rizzo).

1631-0705/$ – see front matter
http://dx.doi.org/10.1016/j.crhy.2012.07.002

presence of static electromagnetic fields may induce a response from the medium which depends on the static field strength. This means that ϵ and μ are not constants, but functions of the external static fields and thus can be written as $\epsilon(E, B)$ and $\mu(E, B)$ where E and B are the total electromagnetic fields, both external and associated to the electromagnetic waves propagating in the medium. Therefore, n depends also on E and B. Each nonlinear optical process essentially consists of two parts. The intense light or the external fields induce a nonlinear response in a medium. Then the medium in reaction modifies the optical fields in a nonlinear way. The former is governed by what are called the constitutive equations, and the latter by the Maxwell's equations [2].

It is well known that all media are nonlinear. However, in 1935 and 1936, taking into account quantum effects, it has been shown that vacuum should also be considered as a nonlinear medium. First theoretical formulations of optical nonlinearities in vacuum at the lowest order in the electromagnetic fields have been published by Kochel, Euler and Heisenberg [3–5]. Their starting point is that it is no longer possible to separate processes in vacuum from those involving matter, since electromagnetic fields can create matter if they are strong enough. And even if they are not strong enough to create matter, they will polarize the vacuum due to the possibility of creating virtual matter, essentially electron–positron pairs, and therefore change the constitutive equations [5].

Although the optical nonlinearity of vacuum is well established by quantum electrodynamics theory (QED), it has never been observed experimentally. It is worth mentioning that QED predictions have been widely and successfully tested in bound systems, as in the case of the Lamb shift of the hydrogen atom [6], or in isolated charged particles, as in the case of the electron $(g-2)$ [7]. However, tests of QED prediction for photon behavior are still lacking. Two phenomena have been studied since many years. The first one concerns photon–photon scattering. An evaluation of the cross section can be found in the original paper of Euler and Kochel in 1935 [3]. For photons in the optical region, this cross section $\sigma_{\gamma\gamma}$ is of the order of 10^{-69} m^2. An attempt to observe photon–photon scattering has been reported in Ref. [8]. Proposals to repeat such an experiment in a different configuration have been reported in the framework of the new very energetic laser facilities like ELI [9] and HiPER [10]. The second phenomenon studied to test QED for the photon itself concerns the propagation of photons in external fields. This is the main subject we are dealing with in our group based at the *Laboratoire national des champs magnétiques intenses* (LNCMI) of Toulouse.

In this article we report on our recent experimental activities concerning the magneto-optics of quantum vacuum. In particular, we will present two experiments searching for two different nonlinear effects of vacuum predicted by QED. The first one corresponds to the magnetic linear birefringence of vacuum, also known as the vacuum Cotton–Mouton effect. The second is the vacuum inverse Cotton–Mouton effect which corresponds to the magnetization of vacuum induced by light in the presence of a transverse magnetic field.

As said before, study of photon propagation inside a transverse magnetic field is of utmost importance, in particular to test QED theory for the photon itself. However, it can also test physics beyond the standard model. For example, photons in a magnetic field are predicted to oscillate into weakly interacting massive particles (WIMPs) such as the axion. This hypothetical particle was introduced by Peccei and Quinn to solve the "strong *CP* problem" [11] and it could be a possible constituent of dark matter. We will finish with a presentation of our experiment on this topic.

2. Experimental tests of quantum electrodynamics for the photon itself

2.1. Maxwell's equations and constitutive equations

In vacuum, when no charge density or current density are present, Maxwell's equations can be written in SI units as:

$$\begin{aligned} \nabla \times \mathbf{E} &= -\frac{\partial \mathbf{B}}{\partial t} \\ \nabla \times \mathbf{H} &= \frac{\partial \mathbf{D}}{\partial t} \\ \nabla \cdot \mathbf{D} &= 0 \\ \nabla \cdot \mathbf{B} &= 0 \end{aligned} \tag{1}$$

where

$$\mathbf{H} = \frac{1}{\mu_0}\mathbf{B} - \mathbf{M} \quad \text{and} \quad \mathbf{D} = \epsilon_0 \mathbf{E} + \mathbf{P} \tag{2}$$

In general $\mathbf{P}$ and $\mathbf{M}$ are functions of $\mathbf{E}$ and $\mathbf{B}$, respectively, and they describe the response of a medium to fields. Eqs. (2) are the constitutive equations. In principle, once these equations are known, the expressions of $\mathbf{P}$ and $\mathbf{M}$ are injected in the Maxwell's equations to fully determine the wave propagation.

In the case of interest, the constitutive equations can be obtained using the following relations:

$$\mathbf{D} = \frac{\partial L}{\partial \mathbf{E}} \quad \text{and} \quad \mathbf{H} = -\frac{\partial L}{\partial \mathbf{B}} \tag{3}$$

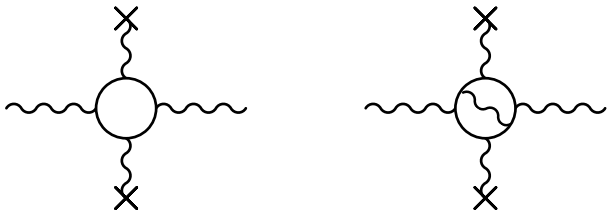

Fig. 1. Left: The Feynman diagram representing the lowest order in the nonlinear effect in vacuum given by Euler and Kochel. Right: Same diagram including the Ritus radiative correction. Solid circular lines represent electron–positron loops, wavy lines represent photons and wavy lines with cross represent ending external fields.

where L is the effective Lagrangian representing the interaction of electromagnetic fields in vacuum. The form of the effective Lagrangian is essentially determined by the fact that it has to be relativistic invariant and therefore can only be a function of the Lorentz invariants F and G:

$$F = \left(\epsilon_0 E^2 - \frac{B^2}{\mu_0}\right) \quad \text{and} \quad G = \sqrt{\frac{\epsilon_0}{\mu_0}}(\mathbf{E}\cdot\mathbf{B}) \tag{4}$$

The general expression can be written in the form:

$$L = \sum_{i=0}^{\infty}\sum_{j=0}^{\infty} c_{i,j} F^i G^j \tag{5}$$

Obviously, one assumes that phenomena involving higher powers of the electromagnetic fields are less probable than phenomena involving lower powers of the electromagnetic fields. So corresponding terms of this series become smaller and smaller and L converges for any value of E and B.

One sees that $c_{0,0}$ does not contribute to the value of D or H. For the sake of simplicity, one can assume that $c_{0,0} = 0$. Moreover, the lowest order terms must give the classical equations $\mathbf{D} = \epsilon_0\mathbf{E}$ and $\mathbf{B} = \mu_0\mathbf{H}$, which gives $c_{1,0} = 1/2$. One finally recovers the usual Maxwell Lagrangian $L_0 = F/2$.

It is important to stress that the magnetic and electric properties of quantum vacuum depend on the form of Lagrangian L which is imposed by Lorentz invariance. Lagrangian terms containing a product of an odd number of electromagnetic fields are not allowed in vacuum. This means that not all the nonlinear effects existing in a standard medium can exist in vacuum. The form of L also indicates that B field and E field of plane waves play an equivalent role as far as nonlinear effect in vacuum is concerned, whereas in standard media, B field is usually neglected and all the effects are ascribed to a $\epsilon(E)$ while $\mu = \mu_0$ [2]. In this sense the vacuum can be considered as a magnetic medium.

At the lowest order in the fields, the Lagrangian established by Heisenberg and Euler [5] can be written as $L_{\mathrm{HE}} = L_0 + L_{\mathrm{EK}}$. L_{EK} is the first-order nonlinear term first calculated by Euler and Kochel [3] which can be represented by the Feynman diagram plotted on the left of Fig. 1.

Moreover, one has to take into account that QED is CP and T invariant. Therefore all the coefficients $c_{i,j}$ with an index j corresponding to an odd number are null. In particular, one gets $c_{0,1} = 0$ and $c_{1,1} = 0$. Finally, L_{EK} can be written as $L_{\mathrm{EK}} = c_{2,0}F^2 + c_{0,2}G^2$. The value of $c_{2,0}$ and $c_{0,2}$ were first given by Euler and Kochel [3]:

$$c_{2,0} = \frac{2\alpha^2\hbar^3}{45 m_e^4 c^5} \quad \text{and} \quad c_{0,2} = 7c_{2,0} \tag{6}$$

with α the fine structure constant, $\hbar$ the Planck constant over 2π and m_e the electron mass.

This result does not take into account all the microscopic phenomena related to the photon–photon interaction in vacuum. Indeed corrections can be calculated taking into account the change induced by the external field in the radiative interaction of the vacuum electrons. Ritus [12] has published in 1976 the corrections to $c_{2,0}$ and $c_{0,2}$. The effective Lagrangian corresponding to the lowest order radiative correction can be represented by the Feynman diagram plotted on the right of Fig. 1. The values of $c_{2,0}$ and $c_{0,2}$ become:

$$c_{2,0} = \frac{2\alpha^2\hbar^3}{45 m_e^4 c^5}\left(1 + \frac{40\alpha}{9\pi}\right) \quad \text{and} \quad c_{0,2} = \frac{14\alpha^2\hbar^3}{45 m_e^4 c^5}\left(1 + \frac{1315\alpha}{252\pi}\right) \tag{7}$$

The Ritus corrections to $c_{2,0}$ and $c_{0,2}$ are α times smaller than the Euler–Kochel value for these two coefficients.

Finally, using Eqs. (2) and (3), one obtains the constitutive equations at the lowest order in the fields:

$$\mathbf{P} = 4c_{2,0}\epsilon_0\mathbf{E}F + 2c_{0,2}\sqrt{\frac{\epsilon_0}{\mu_0}}\mathbf{B}G \tag{8}$$

$$\mathbf{M} = -4c_{2,0}\frac{\mathbf{B}}{\mu_0}F + 2c_{0,2}\sqrt{\frac{\epsilon_0}{\mu_0}}\mathbf{E}G \tag{9}$$

2.2. Vacuum Cotton–Mouton effect

2.2.1. QED prediction

From equations presented in the previous section, one can demonstrate that a transverse magnetic field can induce a linear birefringence in vacuum. This effect is also known as the vacuum Cotton–Mouton effect. It corresponds to the polarization dependence of the velocity of light propagating in the presence of a transverse magnetic field B. The index of refraction $n_\parallel$ for light polarized parallel to the magnetic field is different from the index of refraction $n_\perp$ for light polarized perpendicular to the magnetic field. Values are given in Refs. [13,14]:

$$n_\parallel = \frac{\sqrt{\epsilon_\parallel \mu_\parallel}}{\sqrt{\epsilon_0 \mu_0}} = 1 + c_{0,2}\frac{B^2}{\mu_0} \quad \text{and} \quad n_\perp = \frac{\sqrt{\epsilon_\perp \mu_\perp}}{\sqrt{\epsilon_0 \mu_0}} = 1 + 4c_{2,0}\frac{B^2}{\mu_0} \tag{10}$$

where the symbol $\parallel$ accompanies any quantity related to a light polarization parallel to the static field, and $\perp$ any quantity related to a light polarization perpendicular to the static field. Taking also into account Ritus' corrections for $c_{0,2}$ and $c_{2,0}$, QED predicts:

$$\Delta n = n_\parallel - n_\perp = \frac{2\alpha^2\hbar^3}{15 m_e^4 c^5}\left(1 + \frac{25\alpha}{4\pi}\right)\frac{B^2}{\mu_0} \tag{11}$$

Using the CODATA recommended values for the fundamental constants [15], Eq. (11) gives $\Delta n = (4.031699 \pm 0.000002) \times 10^{-24} B\ (\mathrm{T})^2$.

As we see, the error due to the knowledge of fundamental constants is negligible compared with the error coming from the fact that only the first-order QED radiative correction has been calculated. QED α^4 radiative correction should affect the fourth digit and the QED α^5 radiative correction the sixth digit. Thus measurement of Δn up to a precision of a few ppm remains a pure QED test.

2.2.2. The BMV experimental setup

Several groups attempted to observe and measure vacuum magnetic birefringence [16,17], but this very fundamental prediction has not yet been experimentally confirmed. The principle of main experiments is always the same and follows the proposal in 1979 of Iacopini and Zavattini [18]. The idea is to measure the ellipticity induced on a linearly polarized laser beam by the presence of a transverse magnetic field. A high finesse optical cavity is added in order to increase the optical path in the field. The acquired ellipticity, when the angle between light polarization and the magnetic field B is set to 45°, is given by [19]:

$$\Psi = \frac{2F}{\lambda}\Delta n B^2 L \tag{12}$$

where F is the cavity finesse, λ is the laser wavelength and L is the optical path in the magnetic region. In order to have an induced ellipticity as high as possible, the magnetic field and the optical cavity are critical parameters which have to be optimized.

The BMV experiment, developed at LNCMI in Toulouse so as to measure for the first time the vacuum magnetic birefringence, is detailed in Ref. [19]. Briefly, as shown in Fig. 2, 30 mW of a linearly polarized Nd:Yag laser beam ($\lambda = 1064$ nm) is injected into a Fabry–Pérot cavity consisting of the mirrors M_1 and M_2. The laser frequency is locked to the cavity resonance frequency using the Pound–Drever–Hall method [20]. To this end, the laser is phase-modulated at 10 MHz with an electro-optic modulator (EOM). The beam reflected by the cavity is then detected by the photodiode $\mathrm{Ph_r}$. This signal is used to drive the acousto-optic modulator (AOM) frequency and the piezoelectric actuator of the laser for a fast control and the Peltier element of the laser for a slow control of the laser frequency.

Light is polarized just before entering the cavity by polarizer P. The beam transmitted by the cavity is then analyzed by analyzer A crossed at maximum extinction and collected by a low noise photodiode $\mathrm{Ph_e}$ (intensity of the extraordinary beam I_e). The analyzer also has an escape window which allows us to extract the ordinary beam (intensity I_t) which corresponds to the polarization parallel to P. This beam is collected by the photodiode $\mathrm{Ph_t}$. All the optical components from polarizer P to analyzer A are placed in an ultra high vacuum chamber. Both signals collected by the photodiodes outside the cavity are simultaneously used in the data analysis as follows:

$$\frac{I_\mathrm{e}(t)}{I_\mathrm{t}(t)} = \sigma^2 + \left[\Gamma + \Psi(t)\right]^2 \tag{13}$$

where Γ is the total static birefringence due to mirror intrinsic birefringence and σ^2 is the polarizer extinction ratio. Our polarizers are Glan Laser Prism which have an extinction ratio of 2×10^{-7}. The static birefringence is adjusted thanks to mirrors' orientation in order to have $10^{-3} < \Gamma < 3 \times 10^{-3}$.

The magnetic field is delivered thanks to pulsed coils, which is a novelty as far as linear magnetic birefringence is concerned. The use of pulsed fields for such a kind of measurements has been first proposed in Ref. [21]. In principle, pulsed magnetic fields can be as high as several tens of Tesla, which increases the signal, and they are rapidly modulated which increases the signal to noise ratio. B^2 can be so high that a relative short L is sufficient to obtain a B^2L parameter

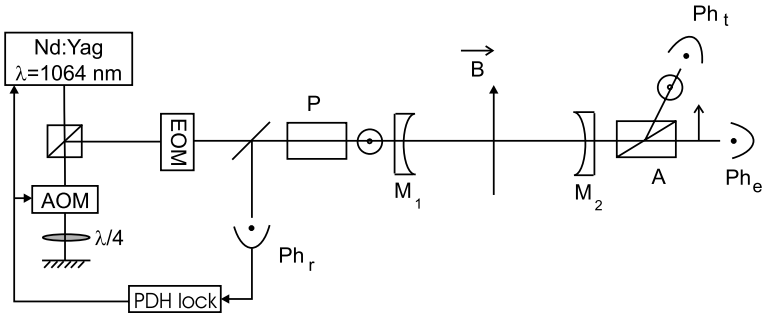

Fig. 2. Experimental setup. An Nd:YAG laser is frequency locked to the Fabry–Pérot cavity made of mirrors M_1 and M_2. The laser beam is linearly polarized by the polarizer P and analyzed with the polarizer A. This analyzer allows to extract the extraordinary beam sent on photodiode Ph_e as well as the ordinary beam sent on photodiode Ph_t. The beam reflected by the cavity analyzed on the photodiode Ph_r is used for the cavity locking. A transverse magnetic field B can be applied inside the cavity in order to study the magnetic birefringence of the medium. EOM = electro-optic modulator; AOM = acousto-optic modulator, PDH = Pound–Drever–Hall.

of a few hundreds of T^2 m. We have been therefore able to mount a table top experiment which is in our opinion the best choice to get high ellipticity sensitivity.

Our present apparatus consists of two magnets, called Xcoils, that have been designed at the LNCMI in Toulouse. The principle of these magnets and their properties are described in details in Ref. [22]. The basic idea is to get the current creating the transverse magnetic field as close as possible of the light path over a length as long as possible to maximize the integral of the square of the field over the magnet length. The coil support is manufactured using G10, a composite material commonly used to deal with high stresses and cryogenic conditions. External reinforcements from the same material are added after winding to contain the magnetic pressure that can be as high as 500 MPa at the field maximum. Like for conventional pulsed magnets, the coil is placed in a liquid nitrogen cryostat to limit heating consequences.

To measure the magnetic field during operation, we measure the current I which is injected in our Xcoil. The form factor B/I has been determined experimentally during the test phase by varying the current inside the Xcoil (modulated at room temperature or pulsed at liquid nitrogen temperature), and by measuring the magnetic field induced on a calibrated pickup coil. The maximum field obtained has been 14.3 T corresponding to a B^2L of about 25 T^2 m. The total duration of a pulse is a few milliseconds and the magnetic field reaches its maximum value within 2 ms.

The stray magnetic field of the magnet should be shielded because it induces systematic effects on the optics and especially on the mirrors which are the elements closest to the magnets. This point is detailed in Ref. [19]. Briefly, two 4-mm-thick copper plates are inserted inside the cryostats to shield the magnetic field outside of the magnet. The field value seen by the cavity mirrors is lower than 400 μT for 14.3 T at the center of the magnet. Taking into account reported values on Cotton–Mouton effects on similar mirrors [23], the magnetic field on the mirror induces a parasitic total ellipticity of the order of 5×10^{-11} rad with a cavity finesse of 500 000. For the moment, this value is much lower than the sensitivity of our experiment.

The other key point of our experiment is the Fabry–Pérot cavity constituting of two interferometric mirrors. Its length is $L_c = 2.27$ m. It has to be large enough to leave a wide space so as to insert our magnets. It corresponds to a free spectral range of $\Delta^{FSR} = c/2L_c = 66$ MHz. In order to increase the induced signal, a finesse as high as possible is essential. To this end, the whole apparatus has been mounted in a clean room since high reflectivity mirrors are very sensitive to pollution. Physicists work therefore fully equipped, as usual, in a clean environment.

Experimentally, the finesse is inferred from a measurement of the photon lifetime τ inside the cavity. For $t < t_0$, the laser is locked to the cavity. The laser intensity is then switched off at t_0 thanks to the AOM shown in Fig. 2 and used as an ultrafast commutator. For $t > t_0$, a typical exponential decay of the intensity of the transmitted ordinary beam is observed as follows:

$$I_t(t) = I_t(t_0)e^{-(t-t_0)/\tau} \tag{14}$$

The photon lifetime is then related to the finesse of the cavity through the relation:

$$\tau = \frac{L_c F}{\pi c} \tag{15}$$

Our best finesse has been obtained using mirrors provided by the *Laboratoire des matériaux avancés* (LMA) of IN2P3, France. We have $\tau = 1.28$ ms corresponding to a finesse $F = 530\,000$ and a cavity linewidth $\Delta\nu = c/2L_cF = 125$ Hz. We summarize in Table 1 the performance of the sharpest known cavities at $\lambda = 1064$ nm. As far as we know, today, our interferometer is the sharpest in the world. Concerning the finesse, the highest ever reached is 1 900 000 as reported in Ref. [26] in a 4-mm-long cavity at $\lambda = 852$ nm. This set a limit to the finesse one can envisage.

Table 1
Summary of performances of some of the sharpest infra-red interferometers around the world, as well as performances of the cavity with the highest finesse ever reached. L_c is the length of the Fabry–Pérot cavity, Δ^{FSR} is its full spectral range, F is the cavity finesse, τ is the photon lifetime, $\Delta\nu$ is the frequency linewidth and $Q = \nu_{laser}/\Delta\nu$ is the quality factor of the interferometer, with the laser frequency ν_{laser}.

Interferometer	Ref.	L_c (m)	Δ^{FSR} (kHz)	F	τ (μs)	$\Delta\nu$ (Hz)	Q
VIRGO	[24]	3000	50	50	160	1000	2.8×10^{11}
PVLAS	[17]	6.4	23 400	70 000	475	335	8.4×10^{11}
LIGO	[25]	4000	37	230	975	163	17×10^{11}
BMV	This work	2.27	66 000	530 000	1280	125	23×10^{11}
Rempe et al.	[26]	0.004	37 500 000	1 900 000	8	20 000	0.18×10^{11}

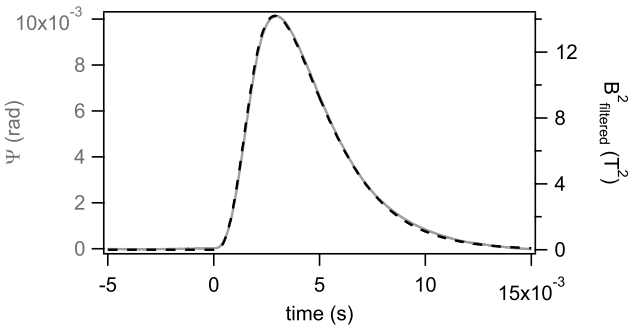

Fig. 3. Cotton–Mouton effect measurement on 32.1×10^{-3} atm of molecular nitrogen. Gray line: Total ellipticity as a function of time. Dashed line: Square of the magnetic field filtered by a first-order low pass filter corresponding to the cavity filtering.

2.2.3. First results

In order to test our apparatus, we have first realized measurements on high purity gas. To this end, the vacuum chamber is connected to several gas bottles through leak valves which allow us to precisely control the amount of injected gas.

Data analysis is explained in details in Ref. [27]. Briefly, the ellipticity induced by the magnetic field Ψ is extracted from Eq. (13). Since the photon lifetime is comparable with the rise time of the magnetic field, the first-order low pass filtering of the cavity has also to be taken into account on the quantity $B^2(t)$ as in Ref. [28]. B^2_{filtered} in the Fourier space is given by:

$$B^2_{\text{filtered}}(\omega) = \frac{1}{1 + i\frac{\omega}{\omega_c}} B^2(\omega) \tag{16}$$

where $\nu_c = \omega_c/2\pi = 1/4\pi\tau$ is the cavity cutoff frequency. The ellipticity is thus proportional to the square of the magnetic field filtered by the cavity and can be written as:

$$\Psi(t) = \kappa B^2_{\text{filtered}}(t) \tag{17}$$

To recover κ, we calculate the correlation between Ψ and B^2_{filtered} for each pulse. A final statistical analysis gives the average value of κ and its standard deviation. Knowing the experimental parameters F, L, λ, one can finally calculate the magnetic birefringence in T^{-2}:

$$\Delta n = \frac{\kappa\lambda}{2FL} \tag{18}$$

In Fig. 3, we plot the square of the magnetic field filtered by the cavity and the measured ellipticity as a function of time obtained with 32.1×10^{-3} atm of molecular nitrogen. We note that both quantities reach their extremum at the same time and their variation can be perfectly superimposed, providing a very precise measurement of magnetic linear birefringence. The signal to noise is so good that the noise is lower than the thickness of the plotted gray line.

Several measurements have been performed at different pressures from 2.1×10^{-3} to 32.1×10^{-3} atm. Our experimental value for nitrogen magnetic birefringence at $B = 1$ T and $P = 1$ atm can be given as $\Delta n_u = (-2.00 \pm 0.08 \pm 0.06) \times 10^{-13}$ $\text{atm}^{-1}\,\text{T}^{-2}$, where 0.08 (resp. 0.06) $\times 10^{-13}$ $\text{atm}^{-1}\,\text{T}^{-2}$ represents the A-type (resp. B-type) uncertainty at 1σ. Our value agrees perfectly well with other existing measurements at $\lambda = 1064$ nm [29,30]. It therefore provides a successful calibration of the whole apparatus.

Once the calibration performed we have evaluated our sensitivity in vacuum which is crucial for us since the goal of our experiment is to measure for the first time the vacuum magnetic birefringence. Our present sensitivity is such that in about 20 ms, i.e. four pulses with $B^2L = 5.3$ T^2 m and $F = 420\,000$, a value on vacuum magnetic birefringence of $\Delta n = (4 \pm 50) \times 10^{-20}$ T^{-2} is obtained, corresponding to a record sensitivity of $\Delta n_s = 7 \times 10^{-20}$ $\text{T}^{-2}/\sqrt{\text{Hz}}$ assuming white noise. For the sake of comparison, the best birefringence limit obtained in vacuum with continuous magnets is $\Delta n \leqslant 2.1 \times 10^{-20}$ T^{-2} with an integration time of 65 200 s [17], corresponding to a sensitivity on Δn of 5.4×10^{-18} $\text{T}^{-2}/\sqrt{\text{Hz}}$. This proves that

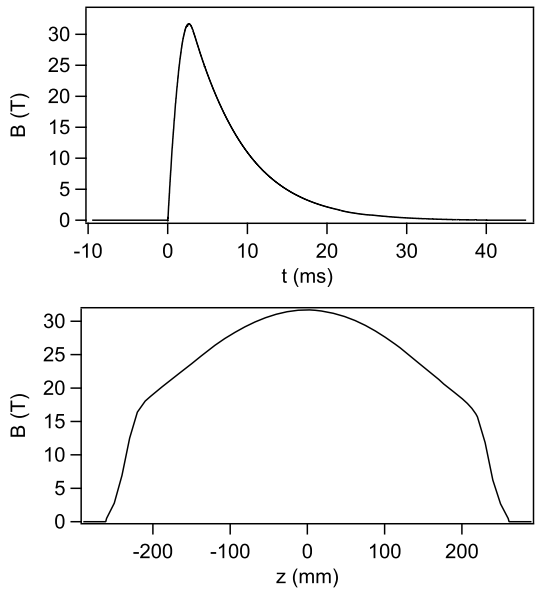

Fig. 4. Measurements of XXLcoil magnetic pulse as a function of time (top) and of spatial profile along the longitudinal z-axis inside one XXLcoil (bottom).

modulation of the effect naturally induced by the pulsed field allows to get a sensitivity that with continuous magnets can only be reached with thousand of seconds of integration time.

2.2.4. Perspectives

Long term perspectives depend on the possibility of having higher magnetic fields. We have designed a new pulsed coil, called XXLcoil, which has already reached a field higher than 30 T when a current higher than 27 000 A is injected. This corresponds to more than 300 T^2 m. In Fig. 4 are plotted measurements of the magnetic pulse as a function of time and the spatial profile for our test XXLcoil. More XXLcoils are under construction and they will be soon operational. BMV experimental final goals are a B^2L in excess of 600 T^2 m as well as a cavity finesse approaching 1 000 000 thanks to very high reflectivity mirrors provided by the LMA. With these experimental parameters, the sensitivity should be improved to $\Delta n_s = 3 \times 10^{-22}\ \mathrm{T}^{-2}/\sqrt{\mathrm{Hz}}$ and the ellipticity due to vacuum magnetic birefringence to be measured should be 5×10^{-9} rad.

If we want to detect vacuum magnetic birefringence with a signal to noise ratio of one in a hundred pulses, i.e. about a few working days, we need a sensitivity of about $\Delta n_s = 3 \times 10^{-24}\ \mathrm{T}^{-2}/\sqrt{\mathrm{Hz}}$. A factor of the order of one hundred should be gained by improving the optical and mechanical stability of the apparatus. We are very confident that eventually the vacuum magnetic birefringence will be observed thanks to our original setup based on pulsed magnets coupled to a very high finesse Fabry–Pérot cavity.

2.3. Vacuum inverse Cotton–Mouton effect

2.3.1. QED prediction

Among nonlinear optical effects in a standard medium, we can cite optical rectification which can be induced by a light beam in the presence of an external magnetic and/or electric field. Such kind of effects are also known as inverse effects with respect to the field induced birefringences. The Inverse Cotton–Mouton Effect (ICME) is a magnetization induced in a medium by a non-resonant linearly polarized light beam propagating in the presence of a transverse magnetic field. This magnetization is proportional to the value of the magnetic field and to the intensity of the propagating electromagnetic waves (see Ref. [2] and references therein). Microscopically, the light-induced dc magnetization arises because the optical field shifts differently the different magnetic states of the ground manifold, and mixes into these ground states different amount of excited states.

Since vacuum is supposed to behave as a standard nonlinear medium, the ICME can be calculated for the quantum vacuum starting from constitutive equation (9) [31]. Two cases are possible: ($\mathbf{E}_\omega \| \mathbf{B}$, $\mathbf{B}_\omega \perp \mathbf{B}$) or ($\mathbf{E}_\omega \perp \mathbf{B}$, $\mathbf{B}_\omega \| \mathbf{B}$), where $\mathbf{E}_\omega$ and $\mathbf{B}_\omega$ are the fields associated to the electromagnetic wave. In the first case one gets:

$$\mathbf{M}_{\mathrm{ICM}\|} = 14 c_{2,0} \epsilon_0 E_\omega^2 \frac{\mathbf{B}}{\mu_0} = 14 c_{2,0} \frac{I}{c} \frac{\mathbf{B}}{\mu_0} \tag{19}$$

while in the second case one obtains:

$$\mathbf{M}_{\mathrm{ICM}\perp} = 8 c_{2,0} \frac{B_\omega^2}{\mu_0} \frac{\mathbf{B}}{\mu_0} = 8 c_{2,0} \frac{I}{c} \frac{\mathbf{B}}{\mu_0} \tag{20}$$

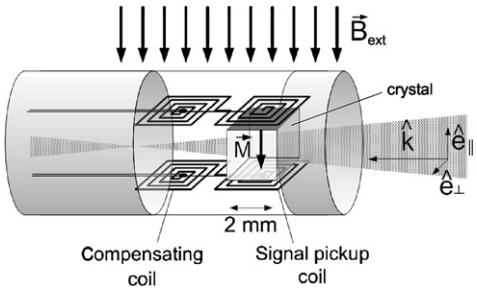

Fig. 5. Detection apparatus: A laser beam crosses the crystal transversal to an applied magnetic field $B_{\rm ext}$. Two sets of pickup-compensating coils monitor the induced crystal magnetization M.

where I is the intensity associated to the electromagnetic wave and where we have used the relation $c_{0,2} = 7c_{2,0}$. In both cases $\mathbf{M}_{\rm ICM}$ is parallel to $\mathbf{B}$.

To have an estimate of the magnetization induced in the case of the quantum vacuum ICME, let's take a 10^{26} W/m^2 laser pulse focused in a vacuum region. This value should be reached at new laser facilities [9,10]. The magnetization to be measured is:

$$\mathbf{M}_{\rm ICM\parallel} \approx 8 \times 10^{-11}\ \mathrm{T} \quad \text{and} \quad \mathbf{M}_{\rm ICM\perp} \approx 4.5 \times 10^{-11}\ \mathrm{T} \tag{21}$$

where we have used the relation $\mu_0 \mathbf{M}\ (\mathrm{A/m}) = \mathbf{M}\ (\mathrm{T})$. These values mean that good sensitivity for magnetization measurements is needed, which is difficult but has already been reached [32].

2.3.2. First observation of ICME in a TGG crystal

The inverse effects have not attracted much of the attention of experimentalists. The first clear observation of the ICME has only been reported very recently by our group with a TGG crystal and it has been reported in Ref. [33]. The apparatus used to this purpose is basically the same that one should set up to observe vacuum ICME at high energy laser facilities.

The laser source was a Q-switched Nd:YAG laser ($\lambda = 1064$ nm) providing 10 ns light pulses of about 0.5 J/pulse. The laser beam passed through two polarizers. The second one fixed the laser beam polarization, while the first one was used to change the laser power delivered to the TGG crystal. A $\lambda/2$ waveplate was placed behind the polarizers to rotate the laser polarization when needed. Folding mirrors and a lens allowed one to deliver and focus the laser beam a few centimeters behind the TGG crystal in order to have a 1.2-mm-diameter spot on the crystal. Crystal dimensions were 2 mm $\times$ 2 mm $\times$ 2 mm. It was subject to a magnetic field $B_{\rm ext}$ parallel to the $[0, 1, 0]$ direction provided by an electromagnet. The field values were in the range 0–2.5 T. The $\mathbf{k}$ vector of light was parallel to the $[0, 0, 1]$ direction, while the polarization of laser light was parallel to the external magnetic field, i.e. parallel to the $[0, 1, 0]$ direction or perpendicular to the external magnetic field, i.e. parallel to the $[1, 0, 0]$ direction.

In Fig. 5 we show a sketch of the detection zone of the experimental apparatus. Changes in the crystal magnetization have been measured using a probe constituted by a double pickup coil, a compensating coil and a signal coil. The signal coil is put in contact with the crystal while the other one is away from the crystal. The double coil is designed in such a way that any signal not coming from the crystal is compensated. Each coil is 2 mm $\times$ 2 mm and the distance between the centers of the two coils is 5 mm. In principle, to avoid signal losses due to returning field lines, the probe should be almost equal in size to the illuminated region and placed as close to it as possible. Each coil has been calibrated by measuring the signal obtained in a known modulated magnetic field. We used two probes of this type, one for the upper side of the crystal and the other one for the lower side of the crystal. The two probes could be rotated to be sensitive to an induced magnetization parallel or perpendicular to the external magnetic field.

The laser pulse is monitored by extracting a small fraction of the beam injected in the crystal with a beam splitter and detecting it with a fast photodiode. The photodiode has been calibrated with respect to an energy meter measuring the pulse energy incident on the crystal.

Since the laser intensity is a function of time, the induced magnetization produces a magnetic flux through the pickup coil. The ICME signal delivered by the pickup coil $V(t)$ is proportional to the time derivative of this magnetic flux and it is thus proportional to the time derivative of the laser intensity:

$$V(t) \propto B_{\rm ext} \frac{\mathrm{d}I}{\mathrm{d}t} \tag{22}$$

This is clearly observed in Fig. 6 where a typical laser pulse together with the corresponding signal detected by one of the two signal coils corresponding to an induced magnetization parallel to the external magnetic field are plotted. We checked that the integrated signal reproduced well the shape of the laser pulse detected by the fast photodiode.

The ICME magnetization of the TGG can be defined as:

$$M = C_{\rm ICM} I B_{\rm ext} \tag{23}$$

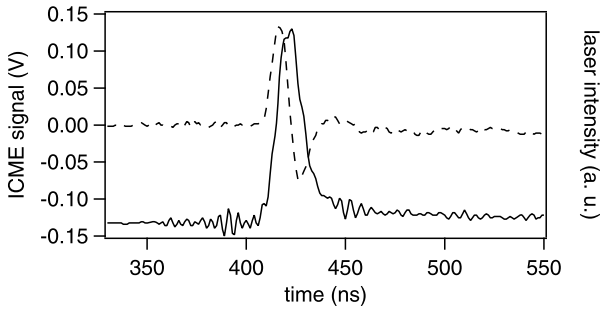

Fig. 6. Magnetization signal (dashed line) and laser pulse (line) as a function of time. The induced signal follows closely the time derivative of the laser intensity.

where C_{ICM} depends only on the medium properties and therefore one may call it the Inverse Cotton–Mouton constant. Measurements as a function of the laser intensity and the external magnetic field show that the magnetic flux density depends linearly on both parameters as expected. Finally, our data indicate that for our TGG crystal $C_{\mathrm{ICM}\parallel} = 8.4 \times 10^{-12}$ $(\mathrm{A,m})(\mathrm{W,T})^{-1}$ and $C_{\mathrm{ICM}\perp} = 5.2 \times 10^{-12}$ $(\mathrm{A,m})(\mathrm{W,T})^{-1}$.

Our results are encouraging to push forward ICME studies in vacuum. Further studies will be realized to optimize the present TGG crystal experiment. In particular, the present sensitivity in magnetization is of the order of 10^{-6} T and thus has to be improved. Then, an experiment will be set up on laser facilities in order to observe for the first time the ICME in gases and finally look for the effect in vacuum.

3. Physics beyond the standard model: axion-like particles

As said in the introduction, study of photon propagation inside a transverse magnetic field can also test physics beyond the standard model since photons in a magnetic field are predicted to oscillate into weakly interacting massive particles (WIMPs) such as the axion. Proposed more than 30 years ago to solve the strong *CP* problem [11], this neutral, spinless, pseudoscalar particle has not yet been detected, in spite of constant experimental efforts.

Most stringent limits on axion or axion-like particle parameters, essentially its mass m_{a} and the coupling constant g of axion to two photons, are given by astrophysical observations [34,35]. However, these limits strongly depend on assumptions for the celestial sources. Purely terrestrial experiments, where axions are produced and then detected on earth, are less sensitive but much more reliable since obtained limits do not depend on any physical model.

Concerning purely terrestrial experiments searching for WIMPs, worldwide efforts are reported in this new scientific domain of low energy particle physics [36] and our team is one of the world leading groups. We have published experimental results improving the limits. The first experiment was realized using a kilojoule laser source provided by LULI, Palaiseau [37].

3.1. Limits on axion-like particle parameters using X-rays

More recently, we have performed a new experiment in the X-ray region, using a beamline coupled with an intense magnetic field at the European Synchrotron Radiation Facility (ESRF), France [38]. Increasing the photon energy in such experiments allows one to test new regions of the m_{a} and g parameter space. Synchrotron light sources provide photons with energy of several tens of keV, much higher than the photon energy available nowadays at other facilities like free-electron lasers.

Our setup corresponds to a photon regeneration experiment, also called “light shining through the wall” experiment [39–41]. The principle is to send a polarized photon beam through a region where a transverse magnetic field is present, and then to stop photons by a wall. Behind this wall, with which the axions do not interact, a second magnetic field region allows the axions to convert back into photons with the same frequency as the incoming ones. Counting these regenerated photons with a suitable detector, one can calculate the axion–photon coupling or put some limits on it.

Our photon regeneration experiment with X-ray beams is detailed in Ref. [38]. Briefly, as plotted in Fig. 7, our setup consists of two superconducting magnets which provide magnetic fields of 3 T over a length of 150 and 97 mm respectively. Each magnet is located separately in the two lead-shielded experimental hutches, EH1 and EH2, respectively, of the beam line. The safety shutter between EH1 and EH2, consisting of a 50-mm-thick lead plate, serves as the wall to block the X-ray beam. The detection system is based on a Ge detector cooled with liquid nitrogen. It combines a high quantum efficiency for the stated photon energies with a reasonable low dark count rate. The X-ray beam is delivered by the beam line ID06 at ESRF. We use two different photon energies, $\omega = 50.2$ keV and 90.7 keV, corresponding to slightly different settings of the X-ray beam line. The incident flux is measured thanks to ionization chambers filled with 1 bar of nitrogen or krypton. During data acquisition, the 30-cm-long krypton filled ionization chamber, located just before the first magnet, is used to precisely monitor the incident flux N_{inc}.

The integration time is about 2 hours for each photon energy in two different configurations, with or without the magnetic fields. Detailed results are presented in Ref. [38]. No excess count above background has been detected. The obtained

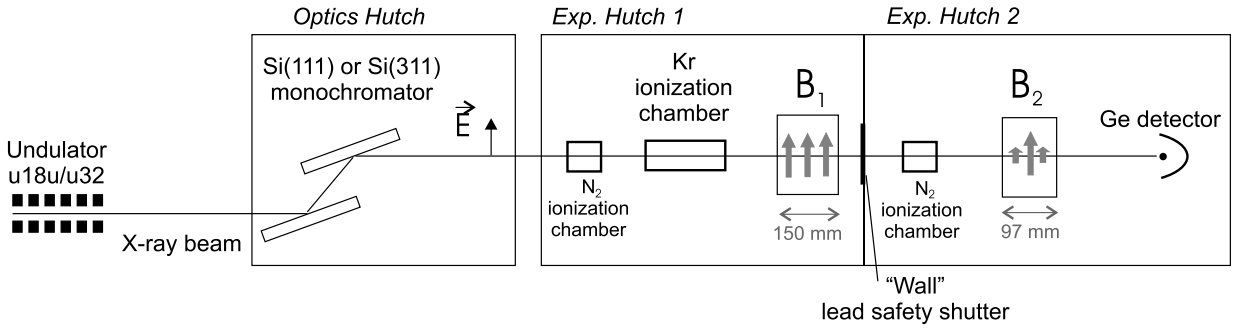

Fig. 7. Experimental setup. The double crystal monochromator is adjusted to select the desired photon energy. The first experimental hutch corresponds to the axion generation area with the transverse magnetic field B_1. The second experimental hutch contains the second magnetic field B_2 which allows the reconversion of axions to photons. These photons are detected by a liquid nitrogen cooled Ge detector with a high quantum efficiency. Ionization chambers placed along the beam path measure the incident flux or serve for alignment purposes. The synchrotron X-rays are polarized parallel to the magnetic fields.

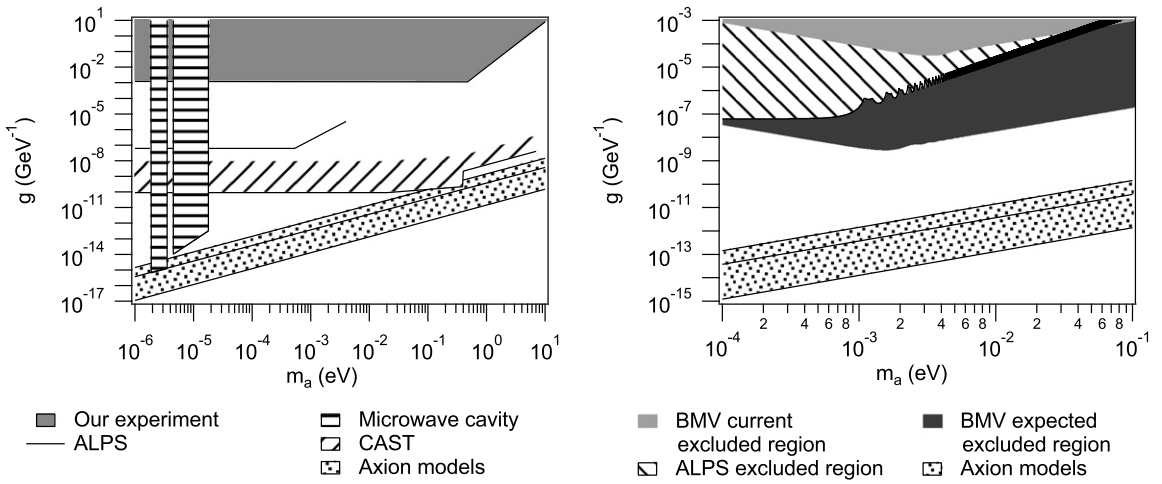

Fig. 8. Left: Limits on the axion–two photon coupling constant g as a function of the axion mass m_a obtained by experimental searches. Our exclusion region obtained at ESRF is presented as the gray area. See the text for more details. Right: Excluded region of the axion in mass–coupling constant space as defined by the BMV setup recent results and when it reaches a resolution of 1.5% of the QED prediction of the quantum vacuum magnetic birefringence.

upper photoregeneration probability at 95% confidence level, corresponding to the error of the regenerated photon rate N_p over the incident photon rate N_{inc}, is $P = 2.2 \times 10^{-15}$ at 50.2 keV, and $P = 9.7 \times 10^{-14}$ at 90.7 keV.

The photon to axion-like particle conversion and reconversion transition probability after propagating in vacuum over a distance z in a magnetic field B may be written as [42]:

$$p(z) = \left| \int_0^z \mathrm{d}z' \Delta_g(z') \times \exp(i\Delta_a z') \right|^2 \simeq \left(\frac{gBL}{2} \right)^2 \left(\frac{\sin(\frac{\Delta_{osc}}{2}L)}{\frac{\Delta_{osc}}{2}L} \right)^2 \tag{24}$$

where $\Delta_g = \frac{gB}{2}$, $\Delta_a = -\Delta_{osc} = -\frac{m_a^2}{2\omega}$ and for a homogeneous magnetic field B over a length L. Finally, the expected count rate due to photoregeneration is:

$$N_p = \eta N_{inc} p_1 p_2 \tag{25}$$

with η the detection efficiency, p_1 the conversion probability in the first magnet, and p_2 the reconversion probability in the second magnet. These equations are correct for $m_a \ll \omega$ [43].

Our experimental sensitivity limit for the axion-like particle to two photon coupling constant versus mass is calculated by numerically solving Eqs. (24) and (25), using the upper photon regeneration probability experimentally measured. Our limits at 95% confidence level are plotted on the left of Fig. 8. Our exclusion region is presented as the gray area. In particular, g is $< 1.3 \times 10^{-3}$ GeV^{-1} for masses lower than 0.4 eV.

We compare our limits to other best limits obtained with laboratory experiments. The best limits obtained on a purely laboratory experiment by the ALPS Collaboration [44] with a 95% confidence level is the region above the solid line. Their limits are given for masses $m_a \ll \omega$, where $\omega \simeq 1$ eV is the photon energy.

Experiments searching for axions of astrophysical origin, such as experiments with microwave cavities (horizontally hashed) [45–47,34] and CAST (diagonally hashed) [35], provide better limits than the purely terrestrial ones. Experiments with microwave cavities, like ADMX, looks for galactic cold dark matter μeV axion conversion into microwave photons in a resonant cavity immersed in a static magnetic field. CAST looks for axions generated in the core of the sun. These axions travel to earth and are converted back into photons of a few keV in a static laboratory magnetic field. Due to the higher photon energy, the CAST limits extend up to masses on the order of a few eV. These limits, however, depend on the model used to calculate the flux of axions to be detected. The critical sensitivity to these models is exposed by the recent proposal of an axion with a 17 meV mass which could explain the observed spectral shape of the X-ray solar emission [48]. In this case, axions coming from the sun's interior would be reconverted into photons near the sun's surface, thus escaping detection by CAST.

Finally, model predictions [49] are also shown as a dotted stripe (line in between: $E/N = 0$ [50,51]). This figure shows that, thanks to the high photon energy, our limits extend to a parameter region where no model independent limits had been set so far. In particular, our experimental results provide limits on the existence of 17 meV axions. The observed low background count rate clearly demonstrates the sensitivity of "shining through the wall" experiments with a synchrotron light source.

3.2. BMV experiment to detect axion-like particles

In the future, our BMV setup will also make an important contribution to the search for axions. The transformation of photons into axions in a magnetic field results in a change of the optical polarization [52]. In the BMV setup, the ellipticity is related to the axion-like particle parameters as follows [53]:

$$\Psi = \frac{F}{\pi}\left(\frac{gB\omega}{m_a^2}\right)^2\left[\frac{m_a^2 L}{2\omega} - \sin\left(\frac{m_a^2 L}{2\omega}\right)\right] \tag{26}$$

On the right of Fig. 8 are shown the limits defined by the BMV setup with current limit at 3σ presented in the previous section together with expected limits when it reaches a resolution of 1.5% of the QED prediction corresponding to the lowest order radiative correction to the main term. By improving the sensitivity of our setup, we also widen the mass and coupling constant range tested by experiments for axions to a level never achieved by terrestrial experiments. As no theoretical consensus exists on the parameters of the axion, enlarging this range can lead to the observation of this elusive particle.

4. Conclusion

Our contribution to this issue of the *Comptes Rendus de l'Académie des sciences* presents an overview of our recent activities. We have developed at the LNCMI of Toulouse in collaboration with other French laboratories like ESRF in Grenoble, LCAR in Toulouse and LMA in Lyon, a wide range of experimental tests whose goal is to study fundamental interactions using high magnetic fields. Magneto-optics of quantum vacuum gives access to phenomena ranging from quantum electrodynamics to physics beyond the standard model. The predicted effects are at such a level that experiments are very challenging. We believe that they will be eventually confirmed thanks to the scientific and technological progress in which magnetic fields will play an essential role.

Acknowledgements

The works presented here could not have been possible without the help of several colleagues of LNCMI, LCAR of Toulouse, LMA of Lyon and ESRF of Grenoble, and in particular G. Bailly, S. Batut, J. Béard, A. Ben-Amar Baranga, F. Bielsa, J. Billette, C. Detlefs, F. Duc, A. Dupays, P. Frings, J.-M. Mackowski, J. Mauchain, C. Michel, M. Nardone, J.-P. Nicolin, L. Pinard, O. Portugall, B. Pinto Da Souza, C. Robilliard, T. Roth, G. Trénec, J. Vigué. We acknowledge the support of the *ANR-Programme non thématique* (ANR-BLAN06-3-139634), *EuroMagNET* and the *Fondation pour la recherche IXCORE*.

References

[1] M. Faraday, Phil. Trans. R. Soc. 1 (1846) 136.
[2] Y.R. Shen, The Principles of Nonlinear Optics, 1st ed., John Wiley & Sons, New York, 1984.
[3] H. Euler, B. Kochel, Naturwissenschaften 23 (1935) 246.
[4] H. Euler, Ann. Phys. 5 (1936) 398.
[5] W. Heisenberg, H. Euler, Z. Phys. 38 (1936) 714.
[6] M. Weitz, et al., Phys. Rev. A 52 (1995) 2664.
[7] D. Hanneke, S. Fogwell, G. Gabrielse, Phys. Rev. Lett. 100 (2008) 120801.
[8] D. Bernard, et al., Eur. Phys. J. D 10 (2000) 141.
[9] See http://www.extreme-light-infrastructure.eu/.
[10] See http://www.hiper-laser.org/.
[11] R.D. Peccei, H. Quinn, Phys. Rev. Lett. 38 (1977) 1440.
[12] V.I. Ritus, Sov. Phys. JETP 42 (1976) 774.
[13] Z. Bialynicka-Birula, I. Bialynicki-Birula, Phys. Rev. D 2 (1970) 2341.

[14] S.L. Adler, Ann. Phys. (N.Y.) 67 (1971) 599.
[15] http://www.codata.org.
[16] S.-J. Chen, H.-H. Mei, W.-T. Ni, Mod. Phys. Lett. A 22 (2007) 2815.
[17] E. Zavattini, et al., Phys. Rev. D 77 (2008) 032006.
[18] E. Iacopini, E. Zavattini, Phys. Lett. B 85 (1979) 151.
[19] R. Battesti, et al., Eur. Phys. J. D 46 (2008) 323.
[20] R.W.P. Drever, et al., Appl. Phys. B 31 (1983) 97.
[21] C. Rizzo, Eur. Phys. Lett. 41 (1998) 483.
[22] S. Batut, et al., IEEE Trans. Appl. Supercond. 18 (2008) 600.
[23] G. Bialolenker, E. Polacco, C. Rizzo, G. Ruoso, Appl. Phys. B 68 (1999) 703.
[24] The Virgo Collaboration, Appl. Opt. 46 (2007) 3466.
[25] M. Rakhmanov, et al., Class. Quantum Grav. 21 (2004) S487.
[26] G. Rempe, R.J. Thompson, H.J. Kimble, Opt. Lett. 17 (1992) 363.
[27] P. Berceau, R. Battesti, M. Fouché, C. Rizzo, Phys. Rev. A 85 (2012) 013837.
[28] P. Berceau, M. Fouché, R. Battesti, F. Bielsa, J. Mauchain, C. Rizzo, Appl. Phys. B 100 (2010) 803.
[29] M. Bregant, et al., Chem. Phys. Lett. 392 (2004) 276.
[30] H.-H. Mei, W.-T. Ni, S.-J. Chen, S.-S. Pan, Chem. Phys. Lett. 471 (2009) 216.
[31] C. Rizzo, et al., Eur. Phys. Lett. 90 (2010) 64003.
[32] N.G. Kalugin, G. Wagnière, Quantum Semiclass. Opt. 3 (2001) S189.
[33] A. Ben-Amar Baranga, R. Battesti, M. Fouché, C. Rizzo, G.L.J.A. Rikken, Eur. Phys. Lett. 94 (2011) 44005.
[34] S.J. Asztalos, et al., Phys. Rev. Lett. 104 (2010) 041301.
[35] E. Arik, et al., J. Cosm. Astropart. Phys. 2 (2009) 8.
[36] J. Jaeckel, A. Ringwald, Ann. Rev. Nucl. Part. Sci. 60 (2010) 405.
[37] C. Robilliard, et al., Phys. Rev. Lett. 99 (2007) 190403.
[38] R. Battesti, et al., Phys. Rev. Lett. 105 (2010) 250405.
[39] P. Sikivie, Phys. Rev. Lett. 51 (1983) 1415.
[40] A.A. Ansel'm, Yad. Fiz. 42 (1985) 1480;
A.A. Ansel'm, Sov. J. Nucl. Phys. 42 (1985) 936.
[41] K. Van Bibber, N.R. Dagdeviren, S.E. Koonin, A. Kerman, H.N. Nelson, Phys. Rev. Lett. 59 (1987) 759.
[42] G. Raffelt, L. Stodolsky, Phys. Rev. D 37 (1988) 1237.
[43] Natural Lorentz–Heaviside units with $\hbar = c = 1$ are employed throughout.
[44] K. Ehret, et al., Phys. Lett. B 689 (2010) 149.
[45] S. DePanfilis, et al., Phys. Rev. Lett. 59 (1987) 839.
[46] W.U. Wuensch, et al., Phys. Rev. D 40 (1989) 3153.
[47] C. Hagmann, et al., Phys. Rev. D 42 (1990) 1297.
[48] K. Zioutas, et al., in: Proceedings of the 5th Patras Axion Workshop, Durham, 2009.
[49] R.D. Peccei, Lect. Notes Phys. 741 (2008) 3.
[50] J.E. Kim, Phys. Rev. Lett. 43 (1979) 103.
[51] M.A. Shifman, A.I. Vainshtein, V.I. Zakharov, Nucl. Phys. B 166 (1980) 493.
[52] L. Maiani, R. Petronzio, E. Zavattini, Phys. Lett. B 175 (1986) 359.
[53] R. Cameron, et al., Phys. Rev. D 47 (1993) 3707.